SolarPACES 2023, 29th International Conference on Concentrating Solar Power, Thermal, and Chemical Energy Systems

Thermal Energy Storage Materials, Media, and Systems

https://doi.org/10.52825/solarpaces.v2i.906

Published: 28 Aug. 2024

Calcium Manganite Based Materials for Thermochemical Energy Storage in High Temperature Solar Thermal Plants: Materials Screening

Chrysa Pagkoura[1], Georgia Kastrinaki[1], and George Karagiannakis[1]

[1] Chemical Process & Energy Resources Institute, Centre for Research & Technology Hellas (CPERI, CERTH)

Abstract. The urgent need for sustainable energy supply requires maximum exploitation of renewable energy sources. The latter, being of intermittent nature, need to be coupled with efficient energy storage. Solar-thermal power-plants are inherently compatible with thermal storage, which is a cost-efficient method of storing energy for later use but the field is currently dominated by sensible heat molten salts used as heat storage media but with a maximum operating temperature of about 560ºC. Certain ceramic materials, able to induce reversible reduction-oxidation reactions under air flow, are promising alternatives to molten salts because they can withstand much higher temperatures (>1000ºC) and thus can be integrated with high-efficiency air-Brayton thermodynamic cycles. At the same time the chemical energy stored/released during such reduction-oxidation reactions can boost energy storage density by up to 10 times cf. sensible only concepts. In this framework, Ca-Mn-based perovskite compositions were demonstrated to function effectively as energy storage materials. The current work offers insights on material synthesis parameters to achieve relatively high purity Ca-Mn-based compositions and subsequently optimize their redox performance in the course of a preliminary 5-cycle campaign. Moreover, the occurring structural transitions and their corresponding heat effects are also discussed and elaborated upon. This study is the first step towards the, currently in progress, process of synthesising – at multi kg scale – and shaping these compositions into extruded honeycomb-like monolithic structures for subsequent future application in lab- and pilot-scale high temperature thermochemical energy storage systems.

Keywords: Thermochemical Energy Storage Cycles, Redox Materials, Perovskites

1. Introduction

Thermochemical energy storage (TCES) is an emerging concept, widely considered as a potential significant asset for the realization of next generation high temperature CSP plants, provided that suitable integration strategies are defined. TCES can, under certain conditions, provide very high energy storage densities; typically one order of magnitude higher compared to state of the art sensible heat storage concepts (e.g. molten salts). TCES schemes based on reversible reduction-oxidation (redox) reactions, employing suitable metal oxides, are particularly attractive for air-operated solar thermal power plants because the air flow can actually be used during both reduction and oxidation steps, thereby rendering utilization/storage of special gases unnecessary. Moreover, the concept is particularly compatible with high-efficiency air-Brayton thermodynamic cycles. A relatively detailed conceptualization of redox schemes for an envisaged relevant application is provided in [1]. Several studies have been published in the last decade, indicating that aspects like materials cost, toxicity, cyclability and satisfactory

structural stability in the course of multiple redox cycles are of prime importance when considering the future practical implementation of such concepts. Calcium manganite ($CaMnO_3$) based materials can cover the aforementioned requirements and are currently considered as a promising, if not the most promising, candidate. Such compositions, being of perovskite structure, are known to function in a non-stoichiometric fashion upon thermal treatment and reversibly release (i.e. reduction) and absorb (i.e. oxidation) substantial amounts of oxygen without losing their structural integrity. Their function is described by the following simplified non-stoichiometric scheme (pure $CaMnO_3$ as example):

$$\mathrm{CaMnO_3} \leftrightarrow \mathrm{CaMnO_{3-\delta}} + {}^{\delta}/_{2}\,\mathrm{O_2}, \Delta \mathrm{H_{RXN}} = \mathrm{f}(\delta) \quad (1)$$

where δ is the reaction non-stoichiometry and $\Delta H_{RXN} = f(\delta)$ means that reaction enthalpy is actually a function of the non-stoichiometry parameter δ.

The present work, studies the effect of important material-related parameters on purity and redox performance of $CaMnO_3$ based compositions. Performance is assessed here by considering both the material weight changes associated with redox reactions (i.e. δ) and the measured effective amount of heat attributed to the enthalpy of identified chemical phenomena. For the latter and in addition to it, at the end of the manuscript, the sensible heat storage potential is also considered. The parametric study involves aspects such as raw materials' purity, preparation conditions (e.g. synthesis method, firing protocol) and dopants (i.e. Sr, Fe) utilization.

2. Experimental

In the current work, seven in-house synthesized perovskite compositions having the $CaMnO_3$ structure as basis, are presented and comparatively characterized with respect to selected physico-chemical characteristics and their preliminary TCES performance. The performance is assessed with the aid of thermo-gravimetric analysis (TGA) and involves quantification of mass changes due to cyclic oxygen uptake (weight gain) and release (weight loss), as measured during oxidation and reduction respectively. For the calculation of δ values per reaction step (i.e. δ_{red} for reduction and δ_{ox} for oxidation), the following equations are used:

$$\delta_{\mathrm{red}} = (2 \cdot \mathrm{MW_{CaMnO3}} \cdot \mathrm{WeightLoss})/\mathrm{MW_{O2}} \quad (2)$$

$$\delta_{\mathrm{ox}} = (2 \cdot \mathrm{MW_{CaMnO3}} \cdot (1 - \mathrm{WeightLoss}) \cdot \mathrm{WeightGain})/\mathrm{MW_{O2}} \quad (3)$$

where MW_{O2} and MW_{CaMnO3}, stand for the molecular weights of oxygen and perovskite respectively. Naturally, the MW of the perovskite depends on its exact chemical formula and here is adjusted to match the MW of the sample's main phase. The values of weight loss and weight gain, correspond to the (%) mass change recorded per reaction step (i.e. ratio of the absolute mass change, as recorded during each reaction step, to the initial sample mass) and since they are both inherent properties of the material and mutually dependent, reduction and oxidation result into similar δ values.

For selected representative cases, in addition to the TGA results heat effects were also quantified via differential scanning calorimetry (DSC) during heating and cooling. The materials' performance is correlated to the purity of the synthesized materials, as measured with post quantitative X-Ray Diffraction (XRD) analysis and defined by the concentration of $CaMnO_3$. To this end, among the evaluated parameters that may affect the properties of the final product are the precursors' source, the synthesis route employed, the thermal treatment protocols and use of dopants. The samples presented here are also compared to raw Mn_3O_4, which exhibits a known redox performance and can be considered as benchmark material.

2.1 Materials synthesis

The six out of seven in total perovskite samples, were synthesized via solid state synthesis (SSS), which is a simple and scalable method. SSS, involves mixing and thermal treatment of suitable solid reactants/precursors. To facilitate the desired solid state reactions and the formation of targeted mixed oxide phase, the technique involves thorough dry mixing (and inevitably co-milling) of stoichiometric solid reactants' quantities with the aid of a planetary mono mill (FRITSCH, PULVERISETTE 6 classic line) and zirconium oxide grinding media. For the samples presented, the optimum mixing time was determined at 180 min. In Table 1, the main characteristics of the raw materials employed for the SSS method, are summarized.

Table 1. *Main properties of raw materials used in the SSS method.*

Raw material	Purity (wt %)	Identified Phases	d_{50}
$CaCO_3$-1	≥ 99.1%	$CaCO_3$ only	60 μm
$CaCO_3$-2	≥ 98.7%	$CaCO_3$, traces of $(Ca,Mg)(CO_3)_2$	95 μm
$CaCO_3$-3	≥ 89%	$CaCO_3$, $(Ca,Mg)(CO_3)_2$	150 μm
Mn_3O_4-1	> 96%	Mn_3O_4 only	2.0 μm
Mn_3O_4-2	> 98%	Mn_3O_4 only	2.1 μm
Fe_2O_3	> 99%	Fe_2O_3 only	0.5 μm
$SrCO_3$	> 98%	$SrCO_3$ only	5.0 μm

The last composition (Table 2), was prepared by a solution-combustion (SC) technique, which involved dissolution of nitrate salts $Ca(NO_3)_2.4H_2O$ from Fluka and $Mn(NO_3)_2.4H_2O$ from Merck) in distilled water and addition of glycine as fuel (metal ions/fuel ratio = 1), according to a modification of the known Pechini process [2]. All samples were calcined under air from room temperature at 1300ºC for 10h, with an intermediate isothermal step at 800ºC for 6 h [3]. In order to study the effect of more intense thermal pre-treatment, sample #2 was subjected to a second calcination; i.e. once calcined, the sample was crushed and grinded with mortar and pestle and re-calcined, resulting in sample #3 (Table 2). Finally, doped compositions of the $CaB_xMn_{1-x}O_{3-\delta}$ general formula, where B = Fe or/and Sr, were also synthesized (#6 - #7). According to relevant past studies, this substitution can improve thermomechanical stability upon redox cycling compared to the undoped $CaMnO_{3-\delta}$ composition [3-6].

Table 2. *Main properties of raw materials used for the SSS method.*

#	Description	Main phase	$CaMnO_3$ content	Mn & Ca Source	Comments
1	Mn_3O_4-1	Mn_3O_4	> 96wt%	-	*Reactant*
2	$CaMnO_3$-A	$CaMnO_3$	54.5wt%	Mn_3O_4-1, $CaCO_3$-3	SSS one calcination
3	$CaMnO_3$-A2	$CaMnO_3$	88.1wt%	Mn_3O_4-1, $CaCO_3$-3	SSS two calcinations
4	$CaMnO_3$-B	$CaMnO_3$	96.8wt%	$CaNO_3$, $MnNO_3$ & glycine	Solution-combustion technique
5	$CaMnO_3$-Γ	$CaMnO_3$	96.7wt%	Mn_3O_4-2, $CaCO_3$-1	SSS one calcination
6	$Ca_{0.95}Sr_{0.05}MnO_3$	$CaMnO_3$	88.4wt%	Mn_3O_4-2, $CaCO_3$-1	5%mol Sr | 2nd phase: ~3wt% $CaMn_2O_4$
7	$(CaMn)_{0.96}Sr_{0.3}Fe_{0.4}O_3$	$Ca_xSr_{1-x}MnO_3$	44.4wt%	Mn_3O_4-2, $CaCO_3$-2	2.5wt% Fe_2O_3 + 2.5wt% SrO | 2nd phase: ~53wt% $CaMn_2O_4$
8	$(CaMn)_{0.92}Fe_{0.16}O_3$	$Ca_xSr_{1-x}MnO_3$	45.5wt%	Mn_3O_4-2, $CaCO_3$-2	10wt% Fe_2O_3 | 2nd phase $CaMn_2O_4$, ~15wt%

2.2 Samples characterisation / performance evaluation protocol

To identify the composition of synthesized materials and estimate their purity with respect to main phase per case, the samples were analyzed by X-Ray Diffraction (XRD) with the aid of a D8 ADVANCE from Bruker equipped with Cu Ka radiation source from 5–80 2θ angle. The materials were subjected to Thermogravimetric Analysis (TGA) and Differential Scanning Calorimetry (DSC) measurements performed on a Netzsch Jupiter STA 449 F3 setup. The samples were evaluated in the course of 5 consecutive cycles in the temperature range of 300-1100^{o}C, at a heating rate of 5K/min and under 100 ml/min of synthetic air flowrate. For all samples, a buoyancy correction was applied via relevant blank measurements.

3. Results and discussion

3.1 Phase characterization

In Figure 1a, XRD patterns of all materials studied are presented. From the comparison, and as already stated in Table 2, the desired perovskite phase, i.e. $CaMnO_3$, constitutes the main phase for samples #2 - #6 (Table 2). Naturally, sample #1 consists entirely of Mn_3O_4, while samples #7 and #8, are mixtures of $(CaMn)_{0,96}Sr_{0.3}Fe_{0.4}O_3$ & $(CaMn)_{0,92}Fe_{0.16}O_3$ and the $CaMn_2O_4$ spinel phase (marokite). For samples #2 through #6, it is known from literature [3] that the specific phase can occur in a variety of stable crystal systems. The cubic form is considered to be the ideal undistorted one while all the rest, i.e. orthorhombic, tetragonal and hexagonal, are identified as distorted forms of the cubic structure. To distinguish between the crystal systems, Figure 1b focuses only on the peaks appearing in the 2θ angle region of 20–50. The set of peaks marked within this region (101, 121, 220, 112 & 202), identified in samples #2 - #6, corresponds to the orthorhombic crystal system. For samples #7 and #8 in particular, the orthorhombic crystal system co-exists with the secondary phase ($CaMn_2O_4$) detected. For the main phases detected in each sample, the wt% main phase concentrations (Table 2) and corresponding crystallite sizes were calculated. The obtained purity of synthesized samples varied substantially with the synthesis parameters and was in the range of 55-98wt%. In general and expectedly, the higher the purity of $CaCO_3$ and Mn_3O_4 precursors the higher the purity of the synthesized $CaMnO_3$ sample. When comparing the effect of the second calcination step (i.e. $CaMnO_3$-A vs. $CaMnO_3$-A2), it becomes obvious that re-calcination leads to phase purity increase (from ~55% to ~88%). Equally pure products are achieved via the SC method ($CaMnO_3$-B). Doping only with Sr and up to 0.05 molar ratio (Sr:Ca, $Ca_{0.95}Sr_{0.05}MnO_3$) may also lead to relatively high purity product (~90wt%), but so far, further doping seems to adversely affect purity of the final product. Finally, with respect to crystallite size of the main phase, in the case of the non-doped samples the $CaMnO_3$ crystallite is calculated at ~1250Å, while in the case of the two doped samples, the crystallite size drops at ~770Å.

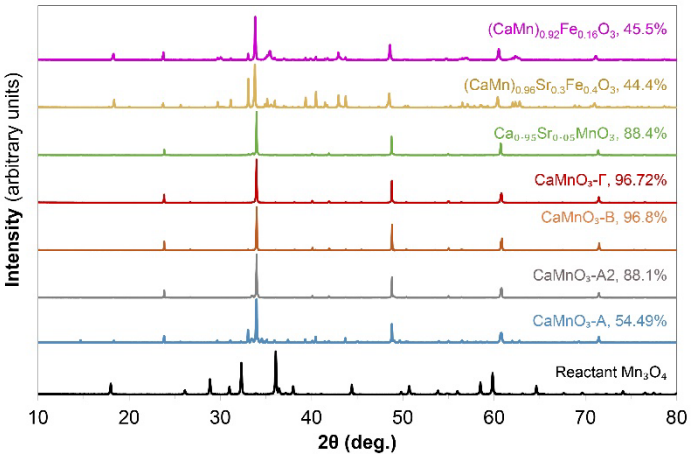

a)

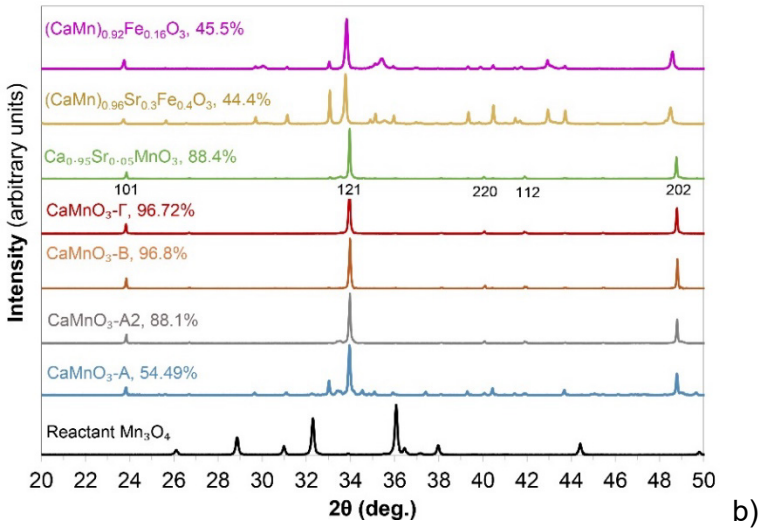

Figure 1. *Comparison of XRD-spectra of all samples; 2θ angles of: a) 10-80 and b) 20-50.*

3.2 Redox performance

Figure 2a presents an exemplary TGA plot of 5 redox thermo-chemical cycles for the $CaMnO_3$-Γ sample. Reduction and associated weight loss occurred in a quasi-continuous manner over a broad temperature range (~800-1100°C) during heating up while oxidation/weight gain took place during cooling down (~1100-650°C). The repeatable weight gain/loss recorded in the course of the 5 cycles indicates no performance degradation. In addition, distinct peaks of heat absorbance and heat release are consistently detected during heating and cooling steps respectively. Figure 2b shows the ones recorded during the 2nd cycle as an example. It must be noted that the corresponding thermochemical endothermal and exothermal phenomena, expressed as two distinct peaks for each, are associated with reversible crystal system transitions [3] and are not explicitly associated with the redox heat effects expected during such a cyclic reaction scheme (i.e. cyclic reaction enthalpy effect) as shown for other redox materials evaluated under similar protocols by TGA/DSC in the past [7]. During heating up, transition from orthorhombic to cubic takes place while during cooling down the inverse change occurs.

The reason why clear redox heat phenomena *per se* are not detected is currently unknown but this observation is consistent in all relevant literature studies assessing perovskites as TCES materials. An explanation could be combination of relatively low reaction enthalpy due to somewhat low δ values (see later in the text) and the very broad temperature range within which the quasi-continuous redox steps occur, contrary to stoichiometric systems (e.g. Co_3O_4/CoO) that are governed by a specific equilibrium temperature [8]. This broad temperature range would cause dilution of heat effects, thereby rendering them undetectable.

In Figure 3, the heat flow of the second cycle for all samples and per reaction step, i.e. (a) heating/reduction and (b) cooling/oxidation, are presented and compared. From the comparison, it is observed that as the $CaMnO_3$ content increases, the heat flow peaks become more evident and so do the corresponding energy content values. The energy content is calculated by integration of the peaks in the course of all 5 cycles and subsequent calculation of average value per sample. Notably, either no (i.e. samples #7 and #8) or substantially lower (sample #6) heat flow is detected in the doped samples thereby indicating that orthorhombic to cubic transition and vice versa is substantially suppressed in such cases. By comparing the $CaMnO_3$-A sample with the 3 doped ones and also considering calculated purity values, it can be safely assumed that the heat flow absence in doped compositions is not entirely attributed to main phase purity but may also relate to orthorhombic structure stabilization due to doping. Work

towards this direction is currently underway. Another interesting comparison is the one between $CaMnO_3$-B and $CaMnO_3$-Γ, as these are two samples with identical purity but synthesized by different methods. The former (SC-synthesized) exhibits heat effects that, despite being of similar profile and value to the ones of $CaMnO_3$-Γ (SSS-synthesized), are actually shifted to somewhat higher temperatures. It is also worth highlighting that the calculated energy content of the best performing $CaMnO_3$ compositions (i.e. $CaMnO_3$-A2, $CaMnO_3$-B and $CaMnO_3$-Γ) is comparable or slightly exceeds the one of benchmark Mn_3O_4.

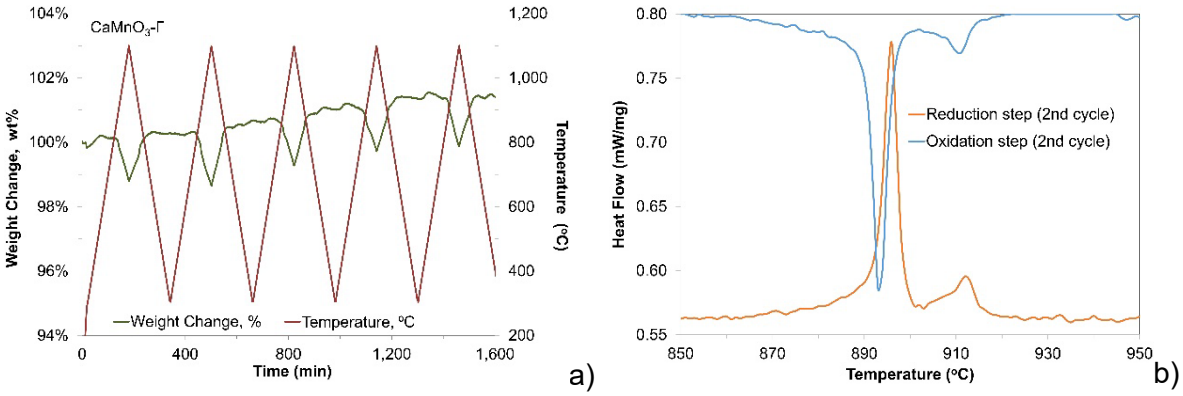

***Figure 2**. Experimental results of the $CaMnO_3$-Γ sample: a) 5 thermal cycles of weight change and temperature as a function of time and b) heat flow recorded during the endothermal and exothermal thermochemical transitions of the 2nd cycle.*

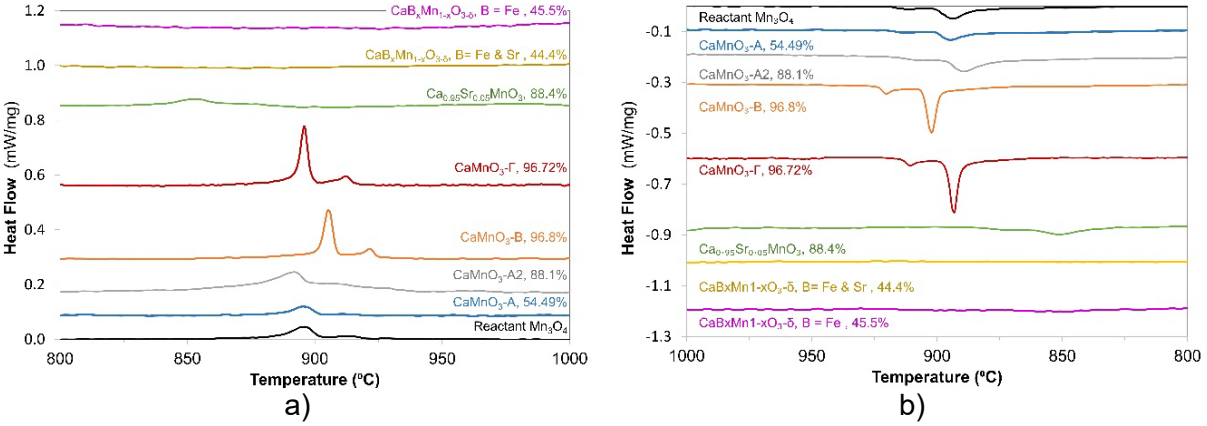

***Figure 3.** Heat flow recorded during the 2nd redox cycle; a) endothermal transition during heating and b) exothermal transition during cooling.*

The calculated average thermochemical energy content and average δ values are quantified in Figure 4. Since, per case, the reduction and oxidation proceed more or less to the same extent, for reasons of simplification and in order to facilitate the comparison of samples, in the graph presented in Figure 4, the average values contain the information of both reaction steps and for all 5 cycles as per the equations:

$$\text{Thermochemical Energy Content (TEC)} = \frac{\text{TEC}_{\text{ox},1}+\cdots+\text{TEC}_{\text{ox},5}+\text{TEC}_{\text{red},,1}+\cdots+\text{TEC}_{\text{red},5}}{\text{n}} \quad (4)$$

$$\delta = \frac{\delta_{\text{ox},1}+\cdots+\delta_{\text{ox},5}+\delta_{\text{red},1}+\cdots+\delta_{\text{red},5}}{\text{n}} \quad (5)$$

All samples, including the three doped ones, exhibit clear redox behaviour and – up to a certain main phase purity value and as indicated by measured δ – the higher the purity, the higher the weight loss/gain / the reduction-oxidation extent (δ). Sample #6

($Ca_{0.95}Sr_{0.05}MnO_3$), which has a purity comparable with the best non-doped $CaMnO_3$ samples, also exhibits similar redox performance and thus it can be claimed that, at least in-principle and for the cases studied here, Sr-doping has no adverse effect on redox behaviour. However, the absence of clear heat effects – as stated above – may be an issue. Combined TCES and sensible heat storage values for samples studied and temperature range considered (i.e. 300-1100°C) were estimated in the range of 660-670 J/g.

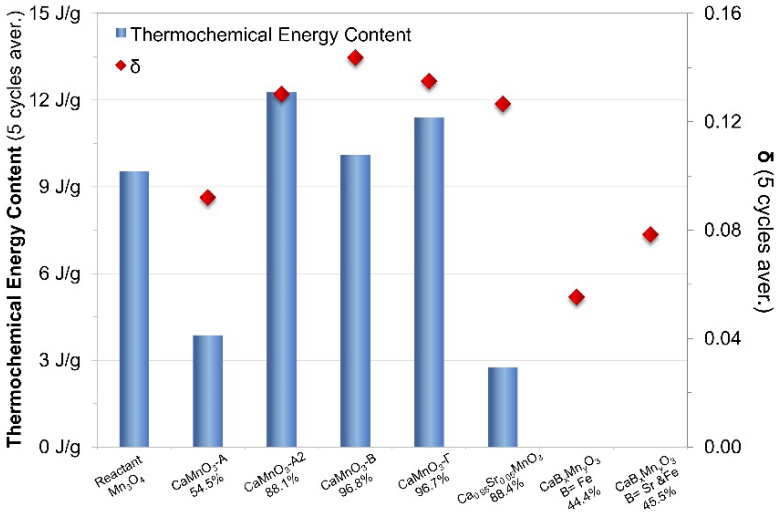

Figure 4. *Average thermochemical energy content and mass changes per sample. The average values refer to both endo- and exo-thermal transitions for all 5 cycles.*

4. Conclusions and future work

With respect to synthesis conditions, the purity of the products is directly dependent on employed reactants' purity and positively affects the redox performance in terms of cyclic weight changes. Heat flow, identified by DSC analysis as two distinct peaks per reaction step in the general temperature range of 840-940°C, seems to be strongly related to the existence or not of the $CaMnO_3$ structure and purity also plays a significant role on the intensity of this phenomenon. Re-calcination improves purity substantially, at least when the once calcined sample is of relatively low purity. Doping with Sr seems to suppress the orthorhombic to cubic structure transition and this may be the main reason for the absence of heat flow in the doped compositions. The range of calculated average non-stoichiometry (δ) values of the compositions studied here and under air flow during reduction-oxidation was determined to be 0.06-0.15. No redox performance degradation was observed in the course of 5 redox cycles conducted as indicated by the repeatable weight gain/loss recorded for all samples, but for brevity actually shown here for one representative $CaMnO_3$ composition. The total amount of heat per cycle during either reduction (heat absorbance) or oxidation (heat release), based on DSC analysis, was calculated to be up to ~12 J/g.

As a next step, already in progress, selected promising compositions among the ones presented here are being and will continue to be synthesized at multi kg scale with the aim of subsequently shaping them into extruded honeycomb-like monolithic structures for future application in lab- and pilot-scale high temperature TCES systems.

Data availability statement

Data will be made available on request.

Author contributions

George Karagiannakis: Conceptualization, methodology, visualization, writing, review and editing, project administration, funding acquisition; **Chrysa Pagkoura**: Conceptualization, methodology, investigation validation, formal analysis, investigation, original draft writing, review and editing, **Georgia Kastrinaki**: Methodology, validation, writing, review and editing.

Competing interests

The authors declare that they have no competing interests.

Funding

This work was performed within the European Union's Horizon Europe research and innovation Projects "ABraytCSPfuture: Air-Brayton cycle concentrated solar power future plants via redox oxides-based structured thermochemical heat exchangers/thermal boosters" under grant agreement No. 101084569 and "HERCULES: High-temperature thermochemical heat storage powered by renewable electricity for industrial heating applications" under grant agreement No. 101104182.

References

1. C. Agrafiotis, M. Pein, A. Eltayeb, L. Klaas, L. de Oliveira, A. K. Singh, M. Roeb, C. Sattler, ''Porous monolithic perovskite structures for high-temperature thermochemical heat storage in Concentrated Solar Power (CSP) plants and renewable electrification of industrial processes'', Conf. Proc., SolarPACES 2023, Oct. 10-13, Sydney, Australia.
2. C. Marcilly, P. Courty, B. Delmon, ''Preparation of Highly Dispersed Mixed Oxides and Oxide Solid Solutions by Pyrolysis of Amorphous Organic Precursors'', J. Am. Ceram. Soc., vol. 53, no. 1, pp. 56-57, 1970, https://doi.org/10.1111/J.1151-2916.1970.TB12003.X.
3. M. Pein, C. Agrafiotis, J. Vieten, D. Giasafaki, S. Brendelberger, M. Roeb, C. Sattler, ''Redox thermochemistry of Ca-Mn-based perovskites for oxygen atmosphere control in solar-thermochemical processes'', Sol. Energy, vol. 198, pp. 612-622, 2020, https://doi.org/10.1016/j.solener.2020.01.088.
4. S.M. Babiniec, E.N. Coker, J.E. Miller, A. Ambrosini, "Doped Calcium Manganites for Advanced High-temperature Thermochemical Energy Storage", Int. J. Energy Res., vol. 40, no. 2, pp. 280-284, 2015, https://doi.org/10.1002/er.3467.
5. L. Imponenti, K.J. Albrecht, R. Kharait, M.D. Sanders, G.S. Jackson, "Redox Cycles with Doped Calcium Manganites for Thermochemical Energy Storage to 1000°C", Appl. Energy, vol. 230, pp. 1-18, 2018, https://doi.org/10.1016/j.apenergy.2018.08.044 .
6. L. Imponenti, K.J. Albrecht, J.W. Wands, M.D. Sanders, G.S. Jackson, "Thermochemical Energy Storage in Strontium-doped Calcium Manganites for Concentrating Solar Power Applications", Sol. Energy, vol. 151, pp. 1-13, 2017, https://doi.org/10.1016/j.solener.2017.05.010.
7. C. Agrafiotis, S. Tescari, M. Roeb, M. Schmücker, C. Sattler, "Exploitation of thermochemical cycles based on solid oxide redox systems for thermochemical storage of solar heat. Part 3: cobalt oxide monolithic porous structures as integrated thermochemical reactors/heat exchangers", Solar Energy, vol. 114, pp. 459-475, 2015, https://doi.org/10.1016/j.solener.2014.12.037nm
8. G. Karagiannakis, C. Pagkoura, E. Halevas, P. Baltzopoulou, A. G. Konstandopoulos, "Cobalt/cobaltous oxide based honeycombs for thermochemical heat storage in future concentrated solar power installations: Multi-cyclic assessment and semi-quantitative heat effects estimations", Solar Energy, vol. 133, pp. 394-407, 2016, https://doi.org/10.1016/j.solener.2016.04.032